Cerebral Cortex, August 2021;31: 3592–3609

https://doi.org/10.1093/cercor/bhab034
Advance Access Publication Date: 16 March 2021
Original Article

ORIGINAL ARTICLE

Variation in Pyramidal Cell Morphology Across the Human Anterior Temporal Lobe

Ruth Benavides-Piccione[1,2,3], Concepcion Rojo[4], Asta Kastanauskaite[1,2] and Javier DeFelipe[1,2,3]

[1]Instituto Cajal, Consejo Superior de Investigaciones Científicas, Madrid 28002, Spain, [2]Laboratorio Cajal de Circuitos Corticales, Centro de Tecnología Biomédica, Universidad Politécnica de Madrid, Madrid 28223, Spain, [3]Centro de Investigación Biomédica en Red sobre Enfermedades Neurodegenerativas (CIBERNED), ISCIII, Madrid 28031, Spain and [4]Sección Departamental de Anatomía y Embriología, Facultad de Veterinaria, Universidad Complutense de Madrid, Madrid 28040, Spain

Address Correspondence to: Ruth Benavides-Piccione, Laboratorio Cajal de Circuitos Corticales, Centro de Tecnología Biomédica, Universidad Politécnica de Madrid, Campus Montegancedo S/N, Pozuelo de Alarcón, 28223 Madrid, Spain.
Email: rbp@cajal.csic.es

Abstract

Pyramidal neurons are the most abundant and characteristic neuronal type in the cerebral cortex and their dendritic spines are the main postsynaptic elements of cortical excitatory synapses. Previous studies have shown that pyramidal cell structure differs across layers, cortical areas, and species. However, within the human cortex, the pyramidal dendritic morphology has been quantified in detail in relatively few cortical areas. In the present work, we performed intracellular injections of Lucifer Yellow at several distances from the temporal pole. We found regional differences in pyramidal cell morphology, which showed large inter-individual variability in most of the morphological variables measured. However, some values remained similar in all cases. The smallest and least complex cells in the most posterior temporal region showed the greatest dendritic spine density. Neurons in the temporal pole showed the greatest sizes with the highest number of spines. Layer V cells were larger, more complex, and had a greater number of dendritic spines than those in layer III. The present results suggest that, while some aspects of pyramidal structure are conserved, there are specific variations across cortical regions, and species.

Key words: 3D reconstructions, cerebral cortex, dendrites, intracellular injections, layer III, layer V, spines

Introduction

In the cerebral cortex, the pyramidal cells are the most abundant neurons. These cells are the main source of intrinsic excitatory cortical synapses, and their dendritic spines (for simplicity, spines) are the main postsynaptic targets of excitatory synapses. Moreover, they form most intraareal projections and nearly all interareal projections (reviewed in DeFelipe and Fariñas 1992). Pyramidal neurons are located in all cortical layers except layer I and they are commonly categorized according to their projection site (e.g., Jones 1984; White 1989). Pyramidal neurons in distinct cortical regions and in different layers participate in different synaptic circuits, thereby segregating particular cortical functions (for review, see Barbas 2015; D'Souza and Burkhalter 2017; Rockland 2019). There are notable differences in the structure of pyramidal cells between layers, cortical areas, and species, with such differences thought to be critical for the functional specialization of the cortical areas (e.g., Elston and Rosa 1997; Jacobs et al. 2001; Bianchi et al. 2011; DeFelipe 2011; Elston et al. 2011; Elston and Manger 2014; Eyal et al. 2014; Mohan et al. 2015; Jacobs et al. 2015, 2018; Benavides-Piccione et al. 2020). Studies of macaque and human cortex have shown marked differences in pyramidal cell structure—both within a given cortical layer and

© The Author(s) 2021. Published by Oxford University Press. All rights reserved. For permissions, please e-mail: journals.permission@oup.com
This is an Open Access article distributed under the terms of the Creative Commons Attribution Non-Commercial License (http://creativecommons.org/licenses/by-nc/4.0/), which permits non-commercial re-use, distribution, and reproduction in any medium, provided the original work is properly cited. For commercial re-use, please contact journals.permissions@oup.com

among cortical areas. For example, the pyramidal cells in granular prefrontal cortex are larger, more branched and more spinous than those in primary motor, visual, and/or auditory cortex (e.g., Jacobs et al. 1993, 2001; Elston et al. 2001; Elston and Rockland 2002). These specializations in pyramidal cell structure endow the neurons with different functional capabilities (reviewed in Elston 2003; Spruston 2008; Luebke 2017).

Recent studies suggest that there is a relationship between macroscale connectome organization and microscale cytoarchitecture in several species including humans (e.g., Scholtens et al. 2014; Barbas 2015; van den Heuvel et al. 2015, 2016; Beul et al. 2017; Garcia-Cabezas et al. 2019; Wei et al. 2019). For example, van den Heuvel et al. (2015, 2016) have reported an association between macroscale connectivity and layer III pyramidal dendritic complexity among human cortical areas. Since many neurological and psychiatric brain disorders display alterations at both the micro- and macroscale level of brain organization, van den Heuvel et al. (2016) have proposed that the study of this micro–macro relationship may help to better comprehend underlying disease mechanisms of neurodegenerative and neurodevelopmental brain disorders. Specifically, the temporal lobe is one of the first affected regions in Alzheimer's disease and temporal lobe epilepsy is one of the most frequent types of human epilepsy. Moreover, the analysis of pyramidal cell structure in this region is of interest because the temporal lobe in humans is disproportionately larger than that of chimpanzees, monkeys, and other species (Rilling et al. 2008; Bryant et al. 2019). Previous studies have demonstrated differences in the degree to which pyramidal cell structure may vary and the difference in size may involve organizational changes in cortico-cortical connectivity (e.g., Elston 2007).

In the present work, we analyzed pyramidal cells at different locations within the human anterior temporal lobe obtained during surgery from patients suffering intractable mesial temporal lobe epilepsy. Specifically, the analysis of the dendritic arborization of pyramidal cells was performed by intracellular injections of Lucifer Yellow in layer III from the temporal pole and the middle (T2) and inferior (T3) temporal gyrus, at several distances from the temporal pole. Additionally, layer V pyramidal neurons were analyzed in T2 region. We found a great inter-individual variability in most morphological variables measured, although some similar geometrical patterns were observed between regions and individuals.

Materials and Methods

Tissue Preparation

A total of seven human cases were used in this study (H153, H155, H205, H206, H213, H263, and H264), with each patient providing informed consent prior to study participation. Tissue was obtained from the anterolateral middle (T2) and inferior (T3) temporal gyri [Brodmann's areas 20, 21, and 38 (Brodmann, 1909; see Zilles and Amunts, 2010)] of patients suffering pharmacoresistant temporal lobe epilepsy (Department of Neurosurgery, 'Hospital de la Princesa', Madrid, Spain; Figure 1 and Table 1). This tissue has been used in previous studies, where detailed information about the cases can be found (Sola et al. 2005; Arion et al. 2006; Kastanauskaite et al. 2009). The tissue was obtained following national laws and international ethical and technical guidelines on the use of human samples for biomedical research purposes. The patients used in this study had normal IQs and, although each had a different history of medications and treatment, they had all been treated with a variety of antiepileptic drugs that affect GABAergic transmission and other neurotransmitter systems. Furthermore, the disease severity was variable (with daily, weekly, or twice monthly seizures) as was the disease duration (from 10 to 42 years). In each case, video-electroencephalogram recordings from bilateral foramen ovale electrodes were used to localize the epileptic focus in mesial temporal structures. Furthermore, subdural recordings with a 20-electrode grid (lateral neocortex) and with a 4-electrode strip (uncus and parahippocampal gyrus) were used at the time of surgery to further identify epileptogenic regions. After surgery, the lateral temporal neocortex of all patients and the mesial temporal structures from all patients except one were available for standard neuropathological assessment. In the case where it was not available (case H264), most mesial structures were absorbed during surgical removal and, therefore, could not be examined. Histopathological examination of the resected tissue showed hippocampal sclerosis in cases H155, H205, H213, and H263, whereas no apparent alterations were found in the hippocampal formation of cases H153 and H206. Only neocortical tissue that showed no abnormal spiking activity (as determined by intraoperative electrocorticography; see Sola et al., 2005; Arion et al., 2006) was included in the study. Furthermore, the cortical tissue used had a normal appearance, based on standard histological preparations (e.g., Nissl staining) and a variety of immunocytochemical techniques to label neurons (e.g., anti-NeuN antibodies), or to label different types of glial cells (e.g., anti-GFAP and anti-Iba1 antibodies, etc.), as well as other antibodies to label GABAergic interneurons (e.g., see DeFelipe et al., 1993; Marco et al., 1996).

After excision, brain tissue was immediately immersed in cold 4% paraformaldehyde in phosphate buffer (0.1 mol/l, pH 7.4; PB). Blocks (approximately 1 cm × 1 cm × 1 cm) at several distances from the temporal pole (Fig. 1) were cut after 2–3 h, and then flat-mounted (e.g., Welker and Woolsey 1974; Elston et al. 1999a), and postfixed in 4% paraformaldehyde in PB for 24 h at 4°C. The tissue was then sectioned (250 µm), parallel to the cortical surface, using a vibratome. For this purpose, we first measured the thickness of the cortical regions at the gyral crowns and cut accordingly to reach the middle of layer III and layer V. By relating these sections to the coronal sections, we were able to identify, using cytoarchitectural differences, the section that contained each cortical layer (see Elston and Rosa, 1997). Briefly, first we cut 250 µm to remove layer I and reach layer II (recognized by the relatively small size and high density of cells). We then cut a further 250 µm to remove layer II such that the next 250 µm section contained layer IIIa (this section was selected to inject the cells). The section that included layer V was 500 µm further down (underlying layer IV that was recognized by the small size and high density of cells). Using this methodology, we are confident that we sampled cells belonging to layers IIIa and Vb.

Intracellular injections

Sections were prelabeled with 4,6-diamidino-2-phenylindole (DAPI; Sigma, St Louis, MO), and a continuous current was used to inject individual cells with Lucifer yellow (8% in 0.1 M Tris buffer, pH 7.4; LY) in cytoarchitectonically identified layers III and V of the anterolateral temporal cortex (Fig. 1). Pyramidal cells were injected at several distances from the apex of the temporal pole; the distances were labeled as: Pole (0–1 cm), T3a (1–2 cm), T3b (2–3 cm), T2b (2–3 cm), T2b V (2–3 cm), and

Table 1 Summary of the clinical data from the epileptic patients and the surgical outcome.

Patient	Age	Sex	Side	Cortical region analyzed	Age at onset, duration (years)	Seizure frequency	Engel scale
H153	28	F	L	Pole, T3a	9, 19	Daily	IV
H155	41	M	L	Pole, T3a	17, 24	1/Week	II
H205	46	M	R	T2b, T3b	4, 42	1/Week	–
H206	44	F	L	T2b, T3b	17, 27	1/Week	–
H213	38	M	L	T2b, T2bV	28, 10	3–4/Week	II
H263	28	M	R	Pole, T2b, T2c	8, 28	Daily	III
H264	48	M	L	T2b, T2bV	19, 29	2/Month	I

Note: F: female; M: male; L: left; R: right. Engel scale for surgical outcome: class I seizure free, class II rare seizures, class III worthwhile improvement and class IV no worthwhile improvement (Engel, 1987).

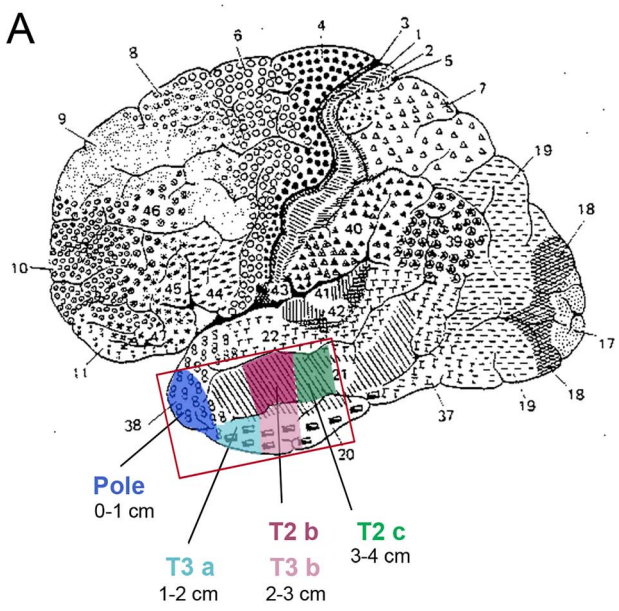

Figure 1. (*A*) Brodmann's map (Brodmann, 1909) in which we highlight the temporal regions analyzed, including areas 38 (Pole), 20 (T3a and T3b) and 21 (T2b and T2c). (*B*) Image of a surgically resected temporal biopsy showing the regions analyzed. Pole (0–1 cm), T3a (1–2 cm), T3b (2–3 cm), T2b (2–3 cm), and T2c (3–4 cm).

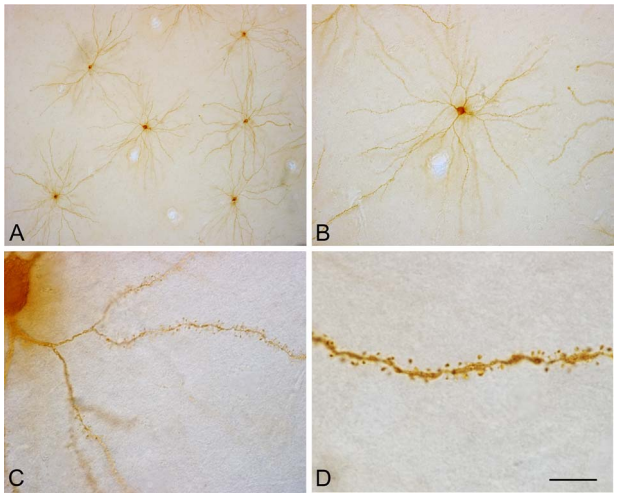

Figure 2. (*A*) Low power photomicrograph showing injected neurons in layer III from T2b of the human temporal cortex, as seen in the plane of section parallel to the cortical surface. (*B–D*) Higher magnification images of cells shown in A, illustrating the spines along the basal dendrites. Scale bar in D corresponds to 220 µm in A, 110 µm in B, 20 µm in C and 10 µm in D.

T2c (3–4 cm). LY was injected by continuous current until the distal tips of each cell fluoresced brightly, indicating that the dendrites were completely filled and ensuring that the fluorescence did not diminish at a distance from the soma (for details of the cell injection method, see Elston and Rosa 1997; Elston et al. 2001; Ballesteros-Yáñez et al. 2010). Following cell injection, the slices were processed with an antibody to LY generated at the Cajal Institute [1:400 000 in stock solution: 2% bovine serum albumin (A3425; Sigma); 1% Triton X-100 (30 632; BDH Chemicals); and 5% sucrose in PB] and then with a biotinylated donkey anti-rabbit secondary antibody (1:200 in stock solution, RPN1004; Amersham Pharmacia Biotech), followed by a biotin–horseradish peroxidase complex (1:200 in PB, RPN1051; Amersham). 3,30-Diaminobenzidine (D8001; Sigma Chemical Co.) was used as the chromogen (Fig. 2). Finally, sections were mounted in 50% glycerol in PB.

Cell Reconstruction and Quantitative Analysis

The Neurolucida package (MicroBrightField, VT, USA) was used to manually three-dimensionally trace the basal dendritic arbor of each pyramidal cell (Fig. 3A,B). The cells were traced by two experts, and one additional expert re-examined the reconstructions searching for possible mistakes. The sections were coded so that neurons were traced blind with regard to the location

of the neuron in the temporal lobe. Only neurons that had an unambiguous apical dendrite were included in this analysis; in total, 274 cells were included. For each cell, the following morphological variables were measured using neurolucida: Area of the basal dendritic arbor (2D convex hull); dendritic length, dendritic nodes and number of dendrites, expressed as total numbers, as a function of the distance from the soma (Sholl analysis), and per branch order; and the cell body area, estimated by measuring the maximum perimeter of the soma. The basal radial extent of each cell refers to the maximum distance reached by the cell (measured by the Sholl concentric outermost sphere) from the cell body. Mean length per branch order refers to the length of dendritic segments (between two consecutive nodes) per order, whereas length per branch order refers to the entire dendritic length that was found per order. The spines were drawn and counted on 21 ± 2 horizontally projecting dendrites per cortical area and case, randomly taken from different cells. Spine density was calculated every 10 µm from the soma to the distal tip of the dendrites while viewed under a x100 oil objective using Neurolucida. Spine density was also calculated as a mean according to the number of spines found in the dendrite divided by the corresponding dendritic length. An estimate of the total number of spines distribution found in the basal dendritic tree of the pyramidal cells was calculated by multiplying the mean number of spines per 10 µm of dendrite with the mean number of branches for the corresponding part of the dendritic tree, from the cell body to the distal tips of the dendrites. The summing of all of these values together accounts for the estimation of the total number of spines (for further details on quantitative analysis see Elston 2001; and Ballesteros-Yáñez et al. 2010; see also Fig. 10).

All statistical analyses were performed using GraphPad Prism version 8 for Windows (GraphPad Software, San Diego, CA, USA) and they are shown in Supplementary Tables 1–27. When morphological parameters were presented as mean values, the Kruskal–Wallis and Mann–Whitney U test was used to compare between the groups. Measurements reported as a function of the distance from the soma were analyzed using two-way analyses of variance (Bonferroni post-tests). Differences were considered to be significant when $P < 0.05$. Measurements are reported as mean ± standard error of mean (SEM), unless otherwise indicated, and are shown in Supplementary Tables 28–30.

Results

A total of 237 layer III pyramidal cells from T2 and T3 temporal gyrus were analyzed at several distances from the temporal pole (Fig. 3A). Additionally, 37 layer V pyramidal neurons were reconstructed in the T2b region (Fig. 3B). Since human cases have been shown to have greater individual variability than any other species studied to date, we have included an analysis at both the individual and the population level.

Layer III Pyramidal Cells

Distribution of Variables per Region and Human Case

We first plotted the size of layer III cells at the various distances from the temporal pole in the different human cases. Cells varied with regard to the size of the basal arbors (Fig. 4A, radial extent; measured as the maximum distance reached by the cell from the cell body; see also basal dendritic field area and soma size in Supplementary Fig. 1A,B; see Supplementary Tables 1–3 for statistical comparisons). The dendritic complexity of cells [measured as the number of dendritic intersections and nodes as a function of the distance from the soma (Fig. 4B,C) and per branch order (Fig. 4D,E)] showed great inter individual variability in many of the morphological measurements (see also other related variables in Supplementary Fig. 1C-E, G, I; Supplementary Tables 4–9 for statistical comparisons). However, some measurements, such as the number of primary and secondary dendrites (Fig. 4D) and the mean dendritic length per branch order (dendritic length between nodes; Fig. 4E), were rather similar between the groups. Spine density (Fig. 4F; calculated as the number of spines found in the dendrite divided by the corresponding dendritic length) and spine density distribution along the distance from soma (Fig. 4G) also showed large differences between the groups (see Supplementary Tables 10 and 11 for statistical comparisons). The highest values were observed in the smallest and least complex cells. Multiplying the mean number of branches per 10 µm of dendrite (Fig. 4B) by the mean number of spines for the corresponding part of the dendritic tree (Fig. 4G) resulted in the estimation of the total number of spines that a cell contains along the distance from soma (Fig. 4H). The sum of these segment estimations is shown as a total number in Fig. 4I. This graph shows that the estimation of spines ranged from ~20.600 to ~6.500. However, when the distribution of these spines (Fig. 4H) was normalized (Fig. 4J), the curves became more similar to each other, showing that the distribution of spines along the dendritic arbor followed a structured pattern regardless of the absolute values.

Distribution of Variables Within a Region

We then plotted cells of the different individuals per region. Figure 5 shows variations between individuals in the T2b region since this was the most sampled region (including five individuals; the remaining regions are found in Supplementary Figs 2 and 3). We found significant differences in the size and branching complexity of cells (Fig. 5A-D; Supplementary Tables 1–9), between cases within a region. There were also significant differences in soma size between individuals (Supplementary Fig. 1B and Supplementary Table 3). Also, some values (the distance from the soma of the maximum number of basal nodes (peak), the number of primary and secondary dendrites, the mean dendritic segment length) remained rather constant (Fig. 5C–E). Interestingly, the individual showing the most complex cells (H264) had low spine density (Fig. 5F,G; statistical comparisons are shown in Supplementary Tables 10 and 11). The estimated total number of spines distribution and total number of spines were also variable between individuals (Fig. 5H,I). However, the normalized distribution of values of the total number of spines from the soma to the end of the dendrite showed that the distribution was quite similar (Fig. 5J), in spite of the large differences found between the different human cases. The distance from the soma of the maximum number of spines was located in all cases at around 90 µm.

Distribution of Variables within Human Cases

To further explore the significance of the results, Figures 6 and 7 show the comparison of the morphological variables distributed per individual cases. These graphs revealed that not all individuals showed a similar trend between regions. For example, in human H153, cells located in the temporal pole were the largest and most complex, whereas in H263 the temporal pole cells were not the largest but had the highest peak of nodes distribution (Fig. 6A–C) compared to posterior regions. However,

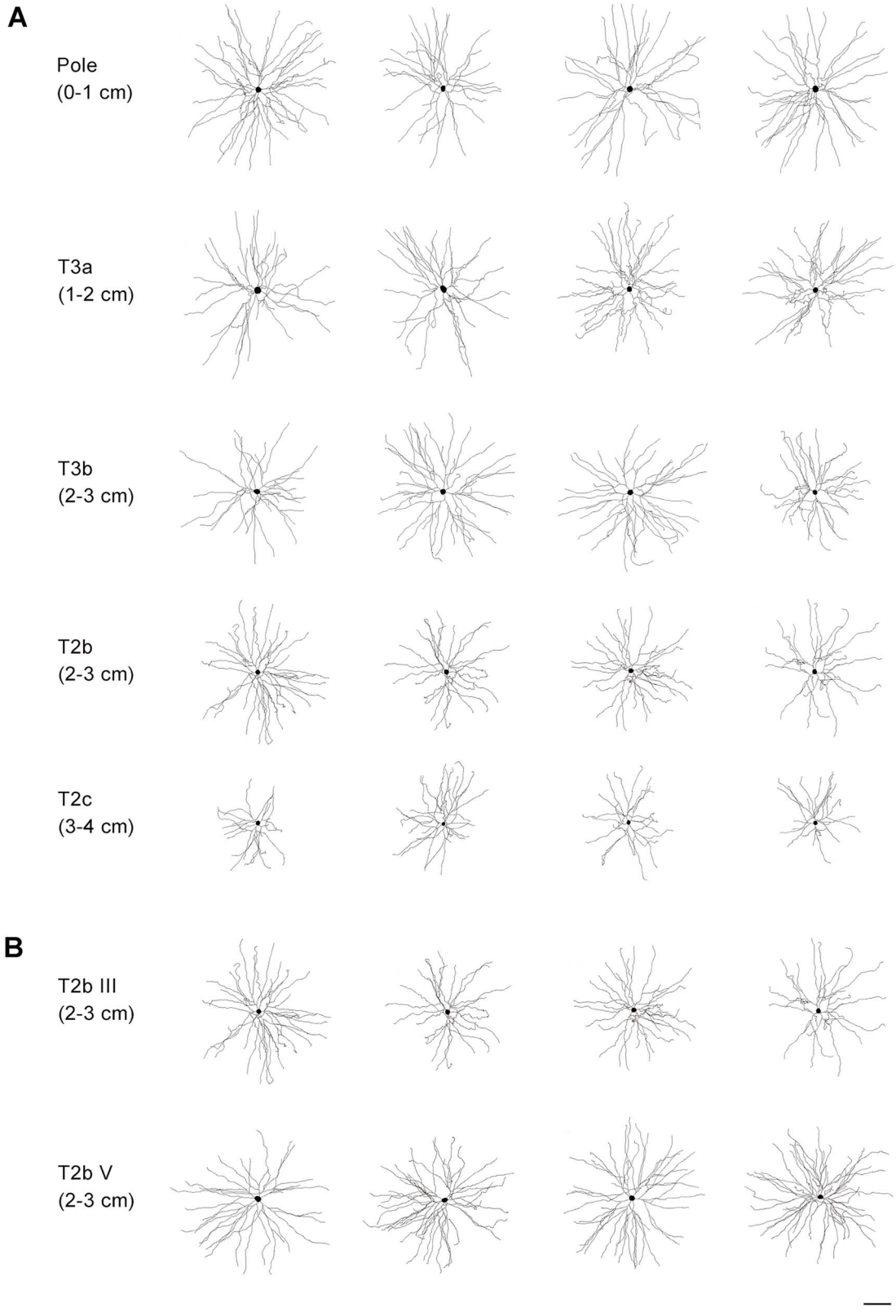

Figure 3. (*A*) Drawings showing some examples of the basal arbors of layer III pyramidal neurons, as seen in the plane of section parallel to the cortical surface, from the middle (T2) and inferior (T3) temporal gyrus at several distances from the temporal pole. (*B*) Drawings showing examples of basal arbors of pyramidal neurons from layer III and V in the T2b region of the temporal gyrus. The cells illustrated are of approximately average size for each group. Scale bar in B corresponds to 100 µm in A and B.

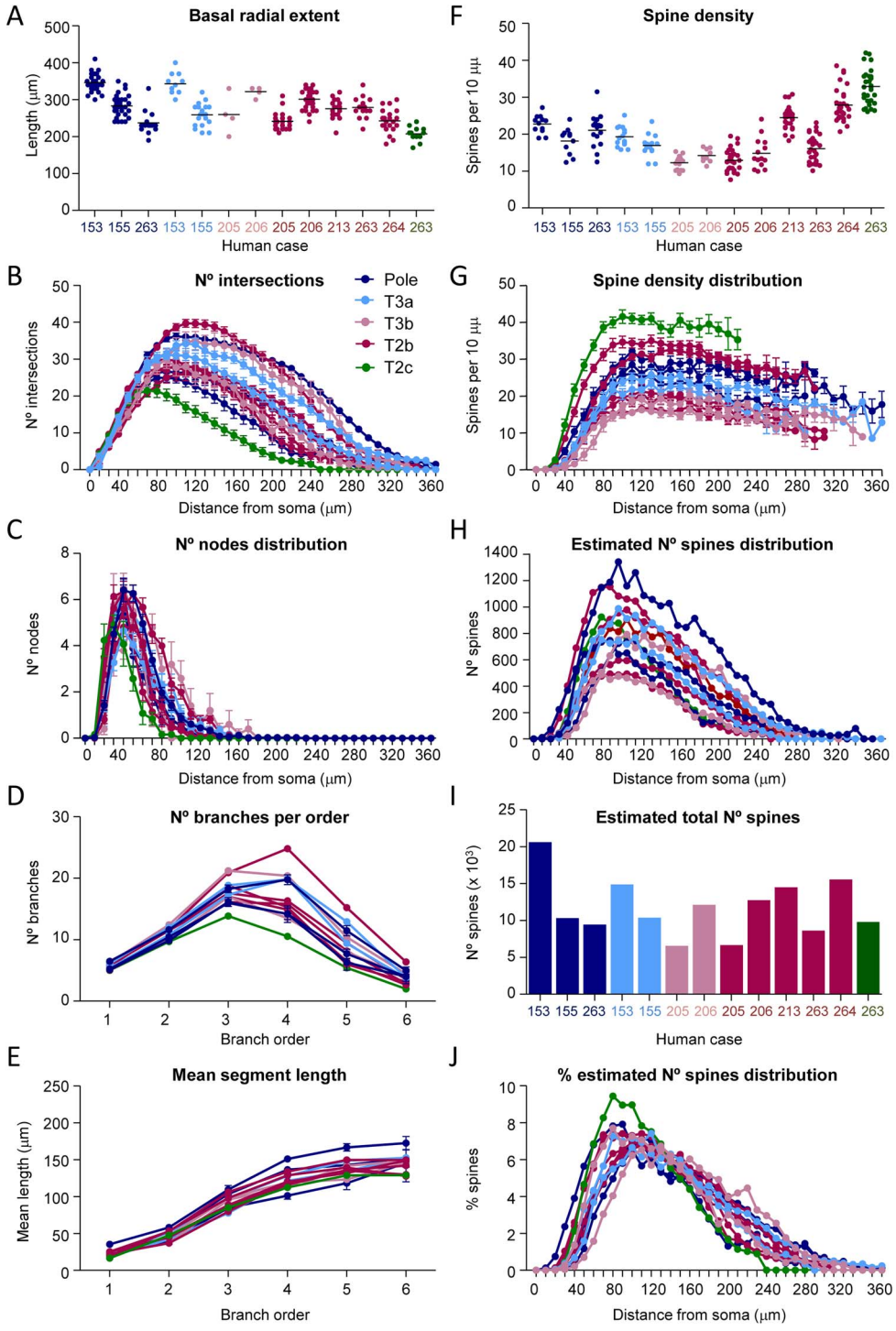

Figure 4. Distribution of variables per region and human case. Graphs showing the distribution of the layer III basal radial extent (*A*), number of dendritic intersections (*B*), number of nodes distribution (*C*), number of branches per order (*D*), mean segment length (*E*), mean spine density (*F*), spine density distribution (*G*), estimated number of spines [*H*, *I*; as a combination of the number of intersections (*B*) and spine density distribution (*G*), expressed as a function of the distance from the soma (*H*) and as a total value (*I*)], and percentage of the estimated number of spines distribution (*J*), per individual analyzed in each cortical region. Note that the percentage of spines distribution is remarkably similar between individuals, despite the differences in branching complexity and spine density. Measurements are reported as mean ± SEM. The statistical significance of the differences is shown in Supplementary Tables 1, 6, 7, 9–11. Additional graphs showing the remaining morphological variables are shown in Supplementary Figure 1.

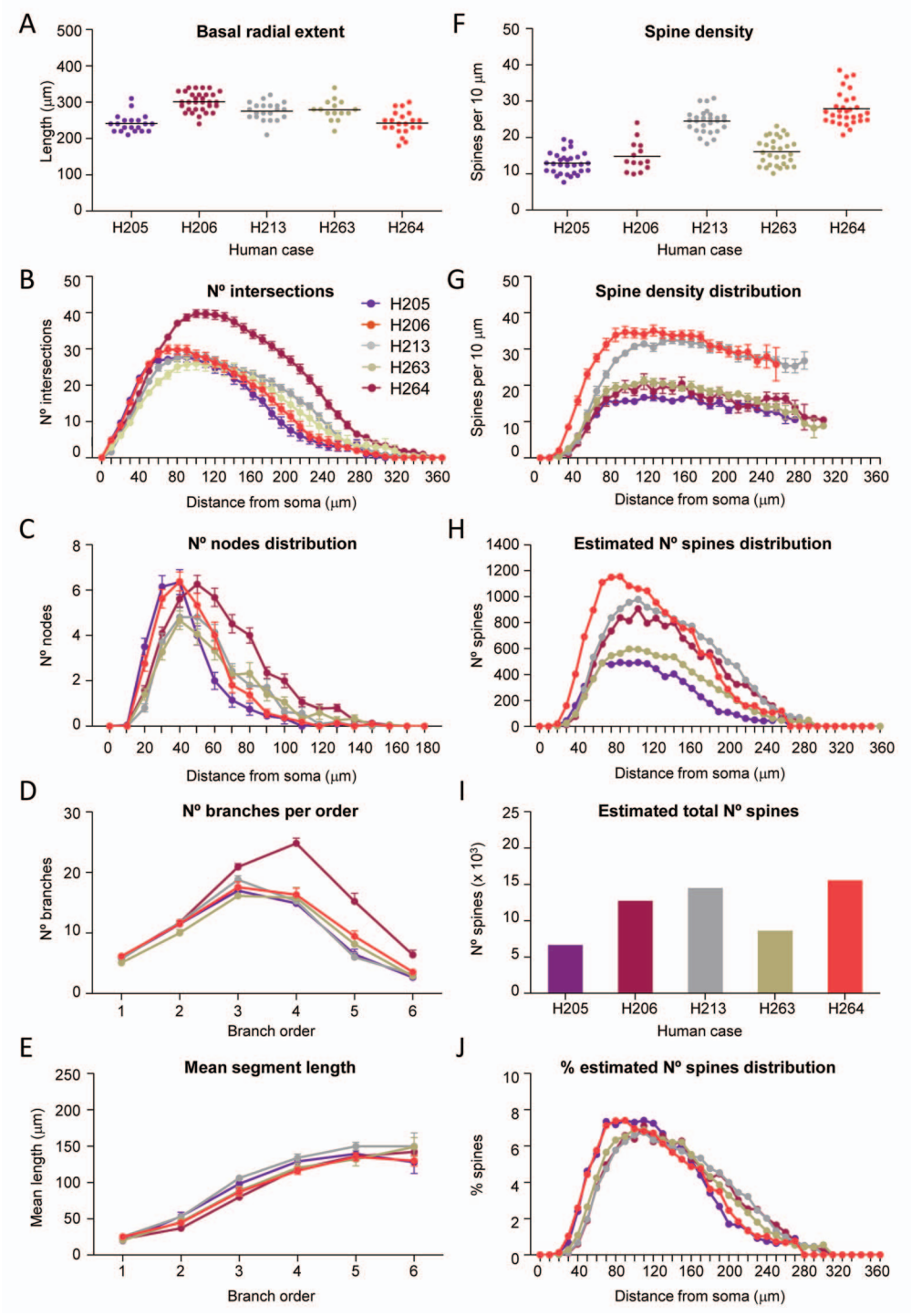

Figure 5. Distribution of variables within a region. Graphs showing the distribution of the layer III basal radial extent (*A*), number of dendritic intersections (*B*), number of nodes distribution (*C*), number of branches per order (*D*), mean segment length (*E*), mean spine density (*F*), spine density distribution (*G*), estimated number of spines distribution (*H*), estimated total number of spines (*I*) and percentage of the estimated number of spines distribution (*J*), for the T2b region of each individual analyzed. Note that the percentage of spines distribution is remarkably similar between individuals, despite the differences in branching complexity and spine density. Measurements are reported as mean ± SEM. The statistical significance of the differences is shown in Supplementary Tables 1, 6, 7, 9–11. Additional graphs showing the remaining morphological variables and regions are shown in Supplementary Figures 1-3.

the statistical analyses showed that most differences in cell size were not significant between regions of the same individual (Supplementary Table 1); likewise, significant differences in the soma size were not found between regions of the same individual (Supplementary Fig. 1B and Supplementary Table 3). The number of intersections per distance from soma (Fig. 6B) showed significant differences in some cases, such as H153 (from 170 µm from the soma), H155 (from 90 to 120 µm from the soma) and H263 (from 140 microns from the soma between pole and T2b and from 90 to 210 microns between T2b and T2c; Supplementary Table 6). The number of nodes distribution was similar between regions in some cases (Fig. 6C), whereas, for example, H263 temporal pole cells showed a significantly higher peak of nodes distribution (see Supplementary Table 7). The number of dendrites per branch order was similar at branch orders 1 and 2, although this number differed at higher orders in some cases (H155, H206, and H263; Fig. 6D). However, the mean dendritic segment length was quite similar between cases (Fig. 6E; Supplementary Table 9; see also other related variables in Supplementary Fig. 4).

Spine density was also variable between individuals (Fig. 7A,B), although differences were significant only between regions of individuals H153 and H263 (Supplementary Tables 10 and 11). The estimated number of spines per distance from soma (Fig. 7C) also showed different distributions of spines between regions of individuals H153 and H263. The total estimated number of spines per individual (Fig. 7D) revealed that there was greater variability in the dendritic complexity and number of spines between individuals than between regions of the same individual. Finally, the normalized distribution of these spines (Fig. 7E) showed that the distribution of spines along the dendritic arbor was similar in all cases except in H263.

Distribution of Variables Between Regions

We then gathered cells per region from different individuals to gain insight into the pyramidal cell morphological variation at a population level. Figure 8 shows significantly larger temporal pole cells compared to T2b and T2c regions (see Fig. 8A and Supplementary Table 12 for statistical comparisons). The branching patterns showed that cells in the temporal pole, T3a, T3b, and T2b were similar in terms of their complexity, and were more complex than the cells in T2c. Specifically, the number of intersections (Fig. 8B and Supplementary Table 13) and length (Supplementary Fig. 5E and Supplementary Table 15) had a similar peak of complexity at ~90 μm from the soma (80 pole, 90 T3a, 100 T3b, and 90 T2b) and ~70 μm from the soma in T2c. Also, T2b regions had statistically fewer intersections than the pole at 220–300 µm from the soma. The number of nodes (Fig. 8C and Supplementary Table 14) had a peak value of ~6 at 40 µm in pole, T3a, T3b, T2b, and ~5 at 30 µm in T2c. The number of primary branches emerging from the soma was very similar between regions (~5) and increased up to branch order 3 in most regions (branch order 4 for region T3a), and then decreased. Region T2c again had the lowest values (Fig. 8D and Supplementary Table 16). The mean length of dendritic segments was remarkably similar in all the groups, with an increase in length from lower to higher orders [order 1–7 (O1–7): mean ± SEM. O1: 22.2 ± 1.5, O2: 48.8 ± 2.41, O3: 94.1 ± 3.50, O4: 123.0 ± 3.32, O5: 138.3 ± 2.97, O6: 147.1 ± 4.93, O7: 152.2 ± 9.08 µm; Fig. 8E and Supplementary Table 17), and it increased in a similar manner from lower to higher orders in all branch orders. See the distribution of length [with the maximum length at branch order 4 in all groups—except for that of the T2c] and nodes [with a maximum number of nodes (~9) at branch order 2 and 3 in all regions except T2c (~7)] in Supplementary Figure 5F, G and Supplementary Tables 18 and 19. Dendritic segments were then further classified according to intermediate segments (meaning a segment that bifurcates) and terminal segments (meaning a segment that ends) (Benavides-Piccione et al. 2020): terminal segments were significantly longer than intermediate segments in all branch orders and cortical regions examined (Supplementary Fig. 5H).

The analysis of spine density (Fig. 8F) revealed that the spine density of cells in T2c was nearly twice that of the other cells (Supplementary Table 20). The distribution of spine density is shown in Figure 8G and Supplementary Table 21. T2b cells, for example, showed spine density values similar to pole and T3a cells. The estimated number of spines per distance from soma (Fig. 8H) showed that all regions except T3b (including the region with the least number of spines and those with the highest spine densities) had similar values of spine distribution up to ~90 µm, where they reached a peak of ~1000 spines. The estimated total number of spines contained within the basal arbor (Fig. 8I) generally increased from posterior to anterior regions (temporal pole: 15359; T3a: 12713; T2b: 12989; T3b: 9148; T2c: 9798 spines). Moreover, the normalized distribution of these spines (Fig. 8J) showed that the distribution of spines along the dendritic arbor followed a structured pattern regardless of the absolute values in all regions except T2c.

Layer III and V Pyramidal Cells

The comparison of layer III and V in the T2b region included 2 individuals (H213 and H264). The analysis of morphological variables per layer and individual revealed that layer V cells were significantly bigger (Fig. 9A; Supplementary Table 1) and had larger number of intersections (statistically significant values were found from 70–100 µm onwards) in both individuals (Fig. 9B; Supplementary Table 6). Furthermore, both individuals in both layers showed similar maximum (peak) number of dendritic nodes at 40 µm (Fig. 9C). Layer V cells from both individuals had a higher number of dendritic nodes from 40 µm onwards compared with layer III cells. This difference was statistically significant from 70 µm onwards (Supplementary Table 7). The number of branches was greater in layer V than in layer III, in both individuals, particularly at higher orders (Fig. 9D), although differences were not statistically significant (Supplementary Table 9). The mean length of dendritic segments was very similar between layers and individuals (Fig. 9E and Supplementary Table 9). The distribution of the dendritic length per branch order showed higher values in layer V cells but similar distribution patterns between the two layers, with the maximum length at branch order 4 (Supplementary Fig. 6F and Supplementary Table 9). The distribution of nodes per branch order was also higher in layer V cells, with similar distribution for all groups, with a maximum number of nodes at branch order 2–3 (~10; Supplementary Fig. 6G and Supplementary Table 9). See also Supplementary Fig. 6A-E for additional values of size and dendritic complexity and Supplementary Tables 2–5 and 8. Mean spine density (Fig. 9F) was not significantly different between the groups (Supplementary Table 10). However, spine density distribution (Fig. 9G) was significantly higher at particular distances from the soma in layer III in the case of one individual but not in the other (Supplementary Table 11). The

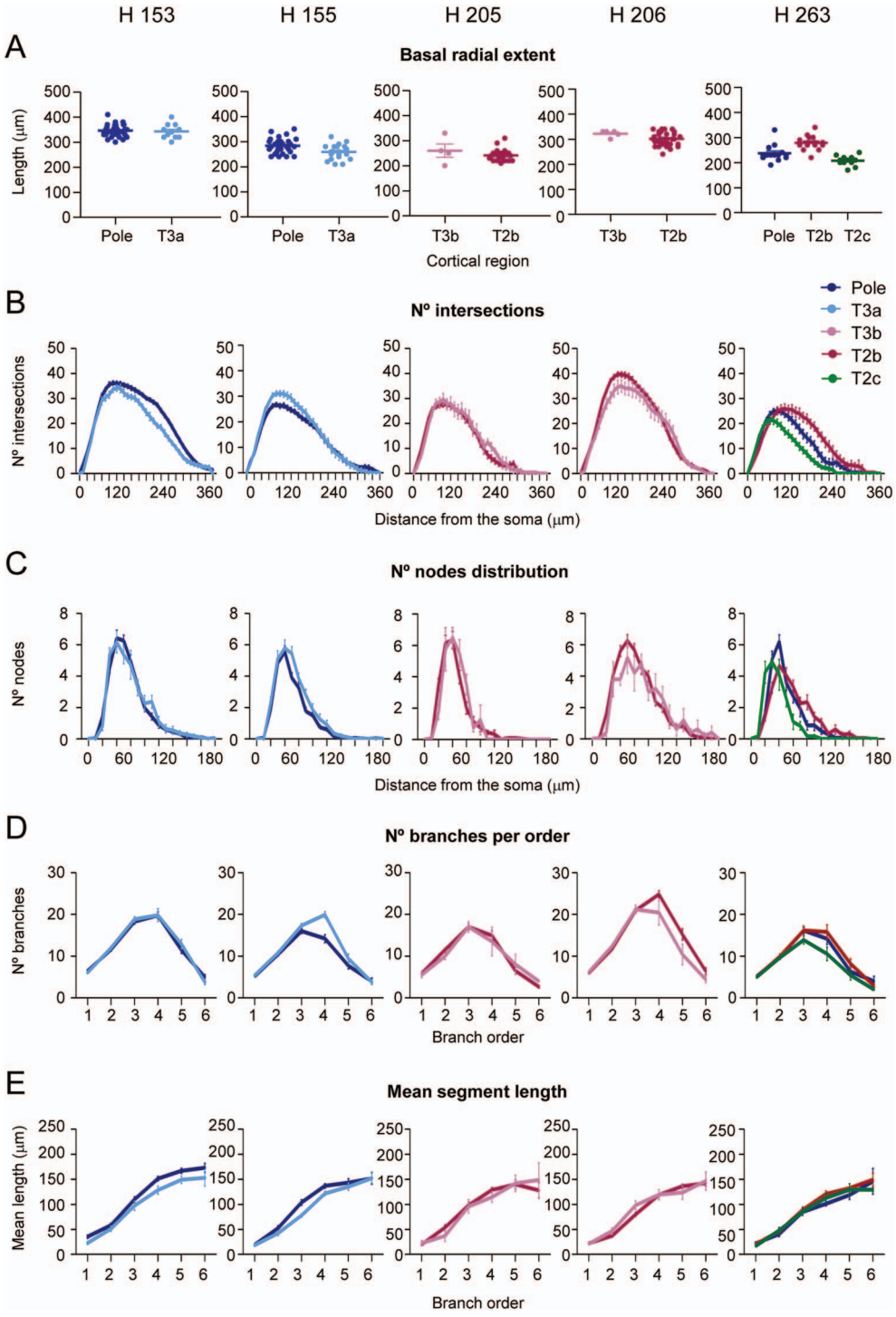

Figure 6. Distribution of variables within human cases (1/2). Graphs showing the layer III basal radial extent (*A*), number of dendritic intersections (*B*), number of nodes distribution (*C*), number of branches per order (*D*) and mean segment length (*E*) from individuals: H153 (first column), H155 (second column), H205 (third column), H206 (fourth column), and H263 (fifth column). Measurements are reported as mean ± SEM. The statistical significance of the differences is shown in Supplementary Tables 1, 6, 7 and 9. Additional graphs showing the remaining morphological variables are shown in Supplementary Figure 4.

combination of the number of dendritic intersections with the distribution of spine density showed greater number of spines in layer V compared to layer III, in both individuals (Fig. 9*H,I*). Nevertheless, the normalized distribution of the number of spines was greater, at a particular distance from soma, in layer III compared to layer V, in both individuals (Fig. 9*J*).

Considering the cells from both individuals together, pyramidal cells were larger and showed greater complexity and a larger number of spines in layer V compared to layer III (Fig. 9A´-J´ and Fig. 10). All differences were statistically significant (Supplementary Tables 22–25. See also Supplementary Fig. 6A´–E´ and Supplementary Tables 26 and 27). The distribution

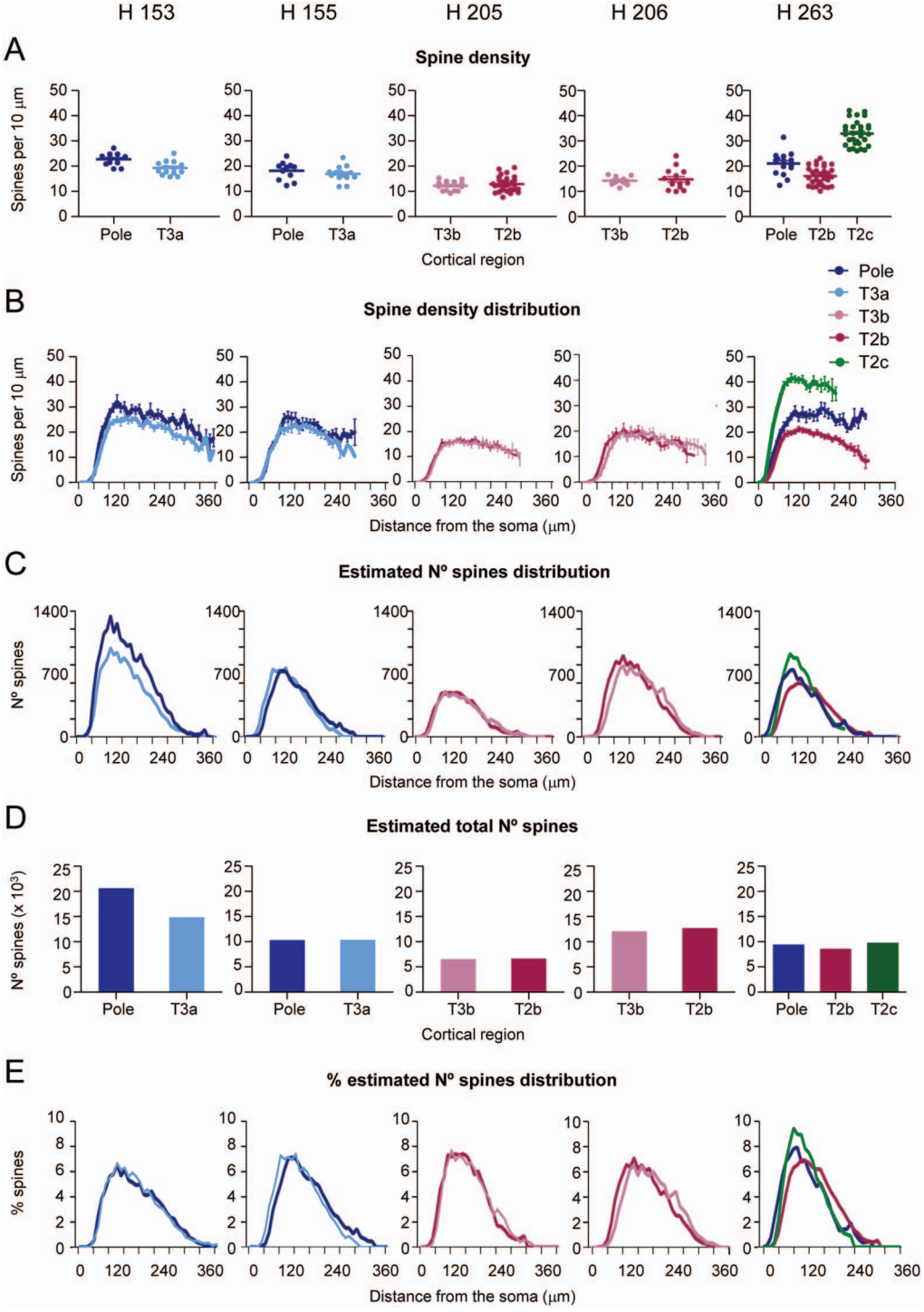

Figure 7. Distribution of variables within human cases (2/2). Graphs showing the layer III mean spine density (*A*), spine density distribution (*B*), estimated number of spines distribution (*C*), estimated total number of spines (*D*) and percentage of the estimated number of spines distribution (*E*), from individuals: H153 (first column), H155 (second column), H205 (third column), H206 (fourth column) and H263 (fifth column). Measurements are reported as mean ± SEM. The statistical significance of the differences is shown in Supplementary Tables 10 and 11.

of the estimated total number of spines as a function of the distance from the soma (Fig. 9H´) shows that values reached higher numbers in layer V (~1200 spines at 110 µm) compared to layer III (~1000 spines at 90 µm). The estimated total number of spines (Fig. 9I´) was higher in layer V (22 279 spines) than in layer III (12 989 spines). By contrast, layer III cells showed a notably higher percentage of spines at a distance of 70–170 µm from the soma (Fig. 9J´), compared to layer V cells.

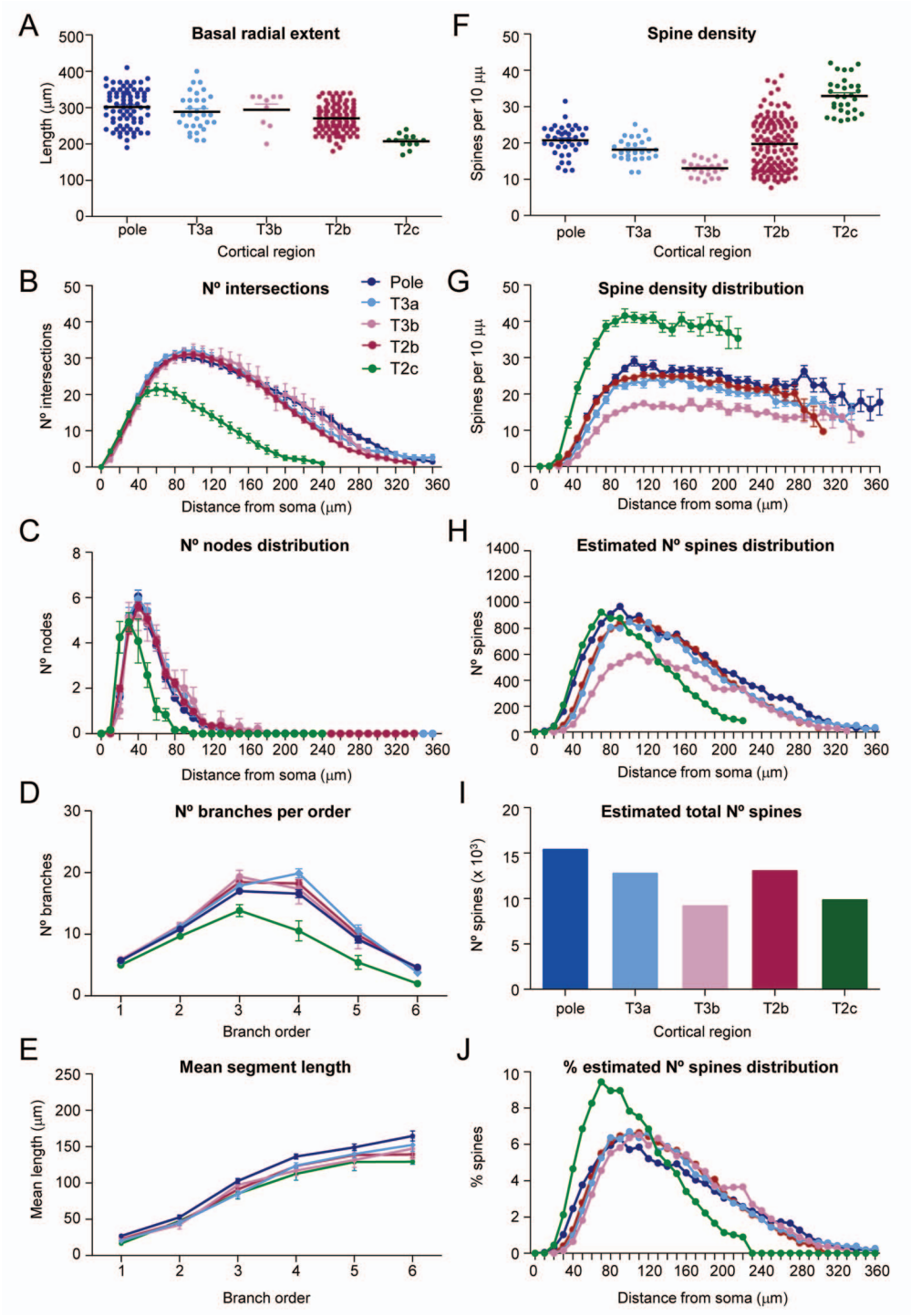

Figure 8. Distribution of variables between regions. Graphs showing the distribution of the layer III basal radial extent (*A*), number of dendritic intersections (*B*), number of nodes distribution (*C*), number of branches per order (*D*), mean segment length (*E*), mean spine density (*F*), spine density distribution (*G*), estimated number of spines distribution (*H*), estimated total number of spines (*I*) and percentage of the estimated number of spines distribution (*J*) per region, taking together cells from the different individuals. Measurements are reported as mean ± SEM. The statistical significance of the differences is shown in Supplementary Tables 12–14, 16, 17, 20, 21. Additional graphs showing the remaining morphological variables are shown in Supplementary Figure 5.

Discussion

This study demonstrates variation in pyramidal cell morphology in the human anterior temporal lobe including the T2 and T3 temporal gyrus at several distances from the temporal pole. The main findings in the present study were the following: 1) there were regional differences in pyramidal cell morphology,

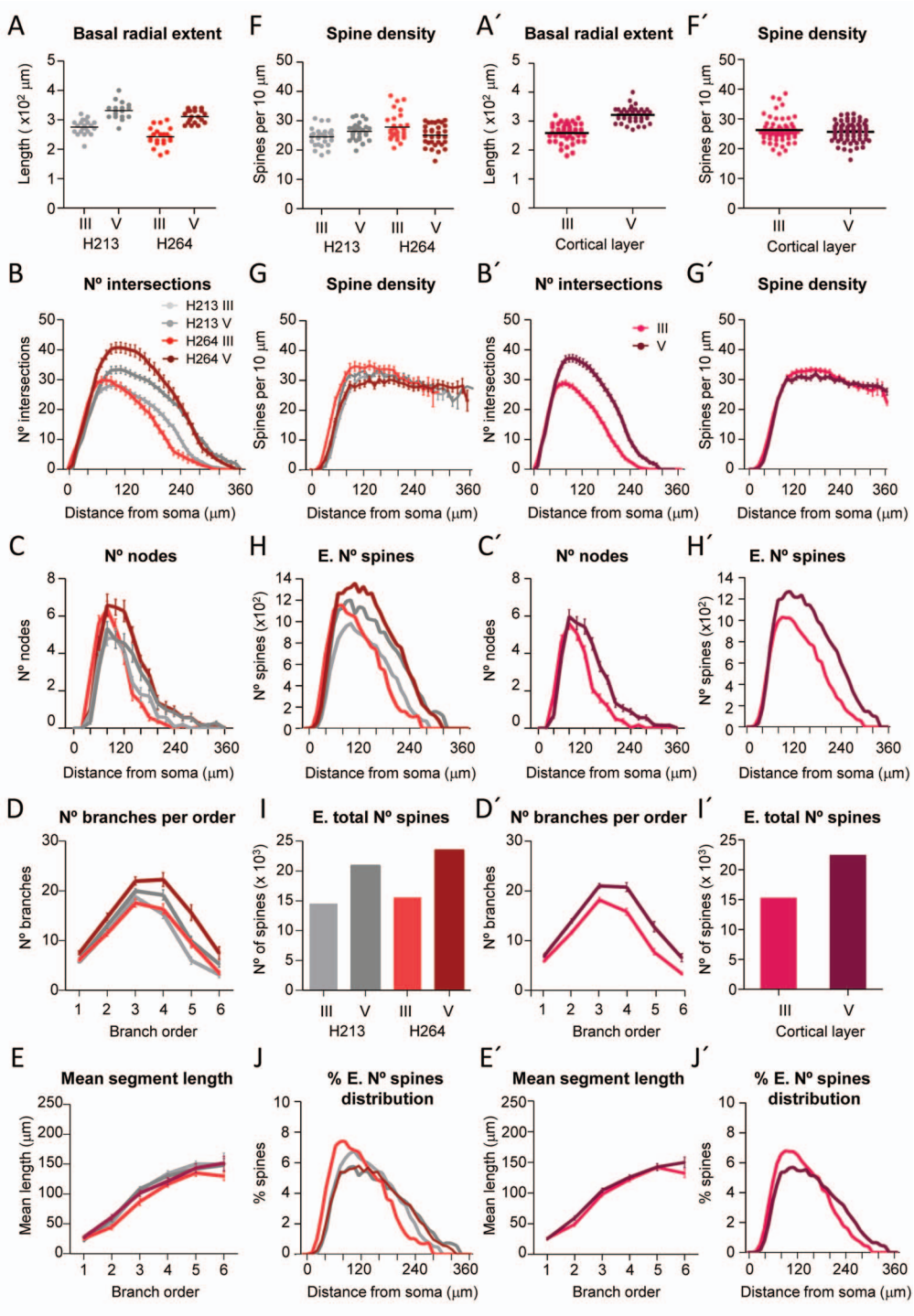

Figure 9. Layer III and V pyramidal cells. Graphs showing the distribution of the basal radial extent (*A*, *A´*), number of dendritic intersections (*B*, *B´*), number of nodes distribution (*C*, *C´*), number of branches per order (*D*, *D´*), mean segment length (*E*, *E´*), mean spine density (*F*, *F´*), spine density distribution (*G*, *G´*), estimated number of spines distribution (*H*, *H´*), estimated total number of spines (*I*, *I´*) and percentage of the estimated number of spines distribution (*J*, *J´*), from layer III and V T2b region for each individual case (*A*–*J*; human cases H213 and H264) and considering the cells from both individuals together (*A´*–*J´*). Measurements are reported as mean ± SEM. The statistical significance of the differences is shown for each individual case (*A*–*J*) in Supplementary Tables 1, 6, 7, 9–11 and per layer comparisons (*A*–*J´*) in Supplementary Tables 22–25. Additional graphs showing the remaining morphological variables are shown in Supplementary Figure 6.

which were greater and showed larger interindividual variability than those reported in other species including non-human primates; 2) the size of the dendritic tree and spine density were key parameters that varied the most among these regions. However, some morphological values and patterns remained rather similar in all cases; 3) the smallest and least complex

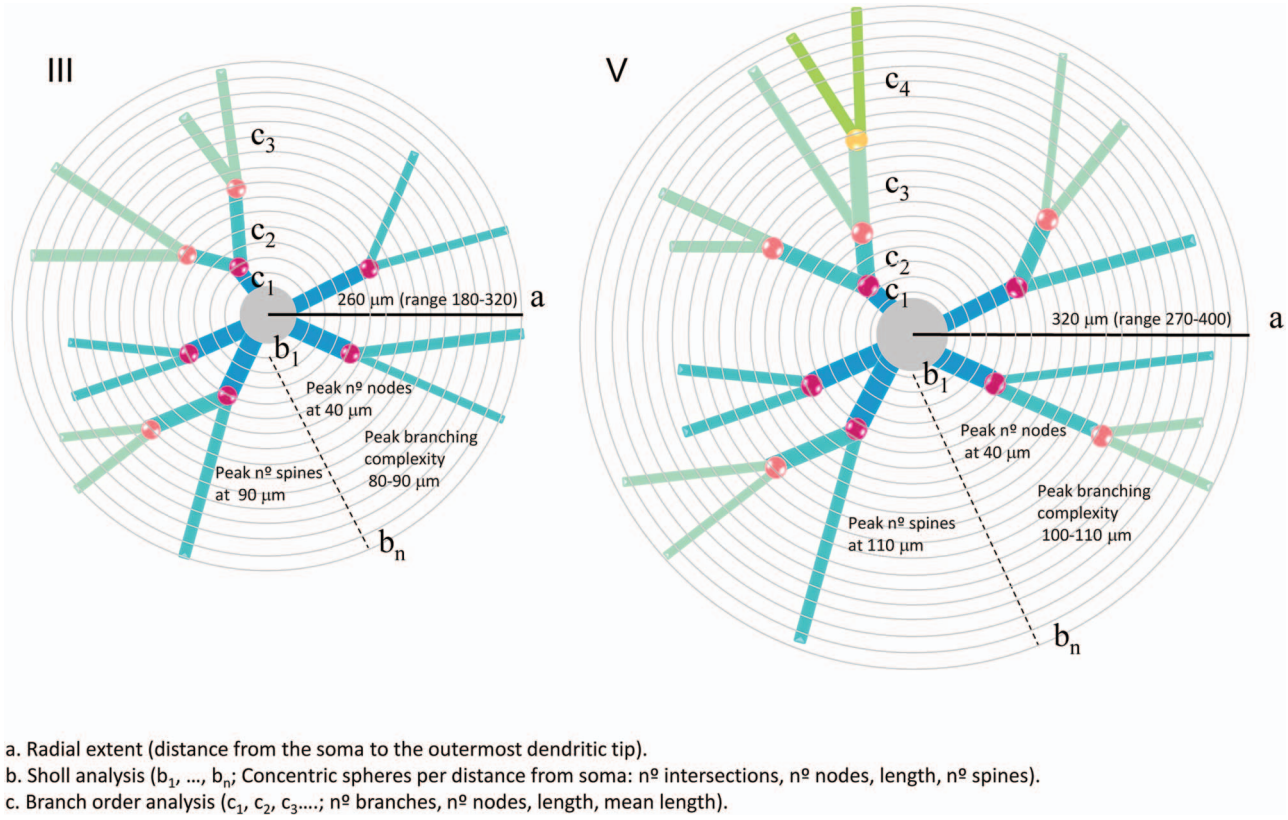

Figure 10. Schematic drawing showing how some morphological variables were analyzed, including (*A*), radial extent; (*B*), Sholl analysis; and (*C*), branch order analysis, using as an example layer III and V pyramidal cells (human cases H213 and H264). Dendritic spines are not represented.

cells in the most posterior region had the greatest spine density, which resulted in a similar number of spines per cell as other regions; 4) pyramidal cells in the temporal pole were the largest, with a relatively high branching complexity and dendritic spine density, which resulted in this area being the one with the highest number of spines; and 5) layer V cells were larger, more complex, and displayed a greater total number of spines than those of the corresponding layer III.

Methodological Considerations

The tissue used in the present study was removed to gain access to the epileptic focus that was located in the mesial structures. In previous studies, it has been shown that the use of biopsy material obtained during neurosurgical treatment for epilepsy, or following the removal of certain brain tumors, represents an excellent opportunity to study the microanatomy of the human brain, since the resected tissue can be immediately immersed in the fixative. Thus, this tissue is lacking possible post-mortem time-induced changes that may occur at both the neurochemical and anatomical levels, which are the main problems associated with the use of brain tissue from autopsies. However, a major drawback is that epileptic patients are heterogeneous in terms of their disease history and it is possible that different medical characteristics of these patients (i.e., differences in medication, severity of the disease, onset, and duration) may modify the brain tissue, although we do not have enough cases to analyze this possibility. We did not find any obvious relation between the larger and more branched cells and age or sex, although the lowest values were observed in the right hemisphere. We are inclined to think that the differences between individuals may simply be due to inter-individual variability. Another aspect that should be considered is that we analyzed a large number of cells, but not all cases included all regions and not all regions included the same number of cells examined. This was due to technical limitations and difficulties in obtaining the same cortical regions (T2 and T3) in all cases. Therefore, further studies with a larger number of individuals would be necessary to obtain more information on the interindividual variability of the pyramidal cell morphological variables. Nevertheless, it is important to bear in mind that the human cerebral cortex is unique in many ways, such as regarding its genetic, molecular, structural, and physiological characteristics (e.g., Elston et al. 2001; Elston 2007; DeFelipe 2011; Hawrylycz et al. 2012; Eyal et al. 2016; Gidon et al. 2020); therefore, research on human brain is fundamental in spite of these limitations. Thus, the present study represents a further step toward the characterization of the human cerebral cortex, but it would be necessary to confirm our findings with a larger number of individuals. What follows is a discussion of the main findings in this study.

As stated above, in the present study, we found great variability within regions between individuals. This has also been observed in other studies on the human cortex (Jacobs and Scheibel 1993; Benavides-Piccione et al. 2005; Benavides-Piccione et al. 2013; Fernández-González et al. 2016; Peng et al. 2019), and in granular prefrontal cortex in other primates (Elston et al. 2011). Notably, the human temporal cortex has been shown to

be one of the regions with the highest interindividual variation in terms of functional connectivity (Demirtas et al. 2019). The morphological variables that varied the most between regions and individuals were the size of cells and dendritic spine density. Functionally, the size and extent of dendritic arbors relate to the sampling strategies of cells and mixing of inputs from multiple sources: cortical and subcortical afferents and local cortical excitatory and inhibitory inputs (e.g., Lund et al. 1993; Malach 1994; Elston et al. 1999a; Elston 2003). Marked differences in the density of spines in different cortical areas, each of which is assumed to receive at least one excitatory glutamatergic synapse, may also influence various aspects related to the integration of inputs along dendrites (for reviews, see Elston 2003, 2007; Spruston 2008; Luebke 2017). These differences may also influence the local summation of post-synaptic potentials or the co-operativity between inputs (e.g., Shepherd et al. 1985). Noticeably, the greatest spine density values were found in the smallest and least complex cells. This has also been clearly observed in the mouse, where the mean density of spines in the relatively small and simple pyramidal cells from the prelimbic cortex is noteworthy in that there is a 2-fold higher density compared to the larger and more complex cells from other cortical areas, which results in a rather spinous basal arbor (Ballesteros-Yáñez et al. 2010). Also, cells in some areas of the primate prefrontal cortex are smaller and have fewer branches than those from the temporal cortex but have a high spine density and, as a result, the estimation of the total number of spines yields higher numbers than in the temporal cortex (Elston 2000; Elston et al. 2011). In the present study, the greatest spine density found in T2c leads the cells in this area to reach quite a high number of spines per neuron. It may be possible that associational areas (such as prelimbic in the mouse study, prefrontal in the primate studies and temporal in the present study), use an increment in spine density as a mechanism to obtain the "sufficient number of spines" needed to integrate associational information in these particular regions. However, the lower branching complexity of these neurons will result in lower compartmentalization of inputs within their dendritic arbors, which will lead to a different summation of inputs (Koch et al. 1982; Spruston 2008; Psarrou et al. 2014; Luebke 2017) of these neurons compared to the other anterior regions. This different structure will lead to different cortical computation of cells between regions.

By contrast, the distribution of some variables—such as the number of primary branches and dendritic segment length—remained similar, both in terms of geometrical arrangement and absolute values, in the different regions and cases. In particular, the mean length of the dendritic segments (length between nodes) that composed the basal arbor was very similar, increasing in length from lower to higher orders in a similar way for all regions and cases studied. This is striking given their variability in absolute values. Also, in spite of their differences in size, dendritic complexity and spine density, the distribution of some variables—such as the distance from soma variables—followed a consistent pattern. This means that although differences in absolute values were found, the distribution can be predicted and approximated to a theoretical distribution. For example, in all cases, the number of branches increased to a peak that was located at approximately one-third of the radial extent of the basal arbors. The peak number of nodes was located at one-seventh of the radial extent of the basal arbors. The distribution of the number of spines along the distance from soma (as a combination of branching complexity and spine density) was quite similar between regions and human cases, in spite of the differences in absolute numbers. Thus, these results suggest that there is a "tuning" between dendritic branching and the number of spines contained therein, which yields a similar distribution of spines between regions. In all cases, the peak spine value occurred at around 90 µm, where the spine numbers ranged from 490 to 1340 (Fig. 4*H*), revealing that the highest numbers of connections are found at this location. In most regions, this peak coincided with the peak of branching complexity. However, in T2c, the peak branching complexity was closer to the soma (at a distance of 60 µm). In all cases, the peak spine density was found at a distance of ~90 µm from the soma. As a result, the normalized distribution of spines as a function of the distance from soma was quite similar between most regions and human cases (Figs 4*J* and 5*J*), although T2c posterior region showed a proportionally higher number of spines at the peak distribution than other regions.

Pyramidal cells in the temporal pole were the largest cells, with a relatively high branching complexity and dendritic spine density, which resulted in this area being the one with the highest number of spines. The variation in size, branching complexity, and spine density of the basal dendritic arborization within the temporal lobe is in line with previous work carried out in human and other species, which has revealed cortical regional specialization (e.g., Lund et al. 1993; Elston and Rosa 1998; Elston et al. 1999a,b, 2001, 2005a,b; Jacobs et al. 2001; Elston 2003; Ballesteros-Yáñez et al. 2010; Bianchi et al. 2013; Mohan et al. 2015; Gilman et al. 2017). Thus, it is likely that the present results reflect differences in neuronal function in the human temporal lobe, suggesting that pyramidal cell specialization is a general organizational principle in the primate brain. Functionally, the larger dendritic arbors allow for greater sampling strategies of cells, more mixing of inputs from multiple sources and greater capacity, as compared with smaller dendritic trees (e.g., Lund et al. 1993; Malach 1994; Elston et al. 1999a; Elston 2003). In addition, the size of the dendritic arbor (its impedance load) strongly modulates the shape of the action potential onset at the axon initial segment and it is accelerated in neurons with a larger dendritic surface area (Eyal et al. 2014). Furthermore, higher branching complexity may determine the degree to which the integration of inputs is highly compartmentalized within the dendritic arbors (Koch et al. 1982; Spruston 2008; Luebke 2017). Indeed, it has been shown that variations in basal total dendritic length, volume and branch number all influence the firing pattern in a predictive manner (Psarrou et al. 2014). Specifically, human cortical neurons show particularly enhanced dendritic compartmentalization due to the large size, dendritic number, and length of human neurons, which has an impact on cortical computation (Eyal et al. 2016, 2018; Beaulieu-Laroche et al. 2018; Gorioununova et al. 2018; Benavides-Piccione et al. 2020; Gidon et al. 2020). The present results suggest that the larger, more branched, more spinous pyramidal cells in the temporal pole may sample a larger number of inputs, compartmentalize such inputs to a greater degree, and integrate these inputs differently from the cells in T2 posterior regions. These findings are consistent with what is known about pyramidal cell function in the human temporal lobe. Specifically, recent work utilizing magnetic resonance imaging has revealed differential results for the modalities described for parcellation at the temporal pole and other temporal areas regarding cortical architecture, function, connectivity, and/or topography (Glasser et al. 2016). It should be noted that the temporal pole is involved in high-level

semantic representation and socioemotional processing, including face recognition and theory of mind (Nakamura and Kubota 1996; for a review, see Olson et al. 2007). Indeed, recent evidence has shown that a circuit model with areal heterogeneity across the cortex is fit to resting state functional magnetic resonance (Demirtas et al. 2019). Also, modeling studies have revealed, by introducing circuit specialization among different cortical areas, that there may be differences in recurrent excitation allowing for the generation of a temporal hierarchy (strong recurrent excitation has been proposed as a mechanism by which prefrontal cortex, for example, could implement "cognitive-type" computations, like information integration and memory-related delay activity; Chaudhuri et al. 2015). In particular, these authors establish a circuit mechanism for "temporal receptive windows" that are progressively enlarged along the cortical hierarchy, suggesting an extension of time integration in decision-making from local to large circuits. Furthermore, Burt et al. (2018) suggest a hierarchical axis linking cortical transcription and anatomy, along which gradients of microscale properties may contribute to the macroscale specialization of cortical function. This relationship between structure and function has also been found in studies on rats and monkeys (e.g., Fujita 2002; Fletcher and Williams 2019), in which it has been claimed that neuronal computations are determined by neocortical location.

The comparison of the present results with data obtained in previous human related areas such as the CA1 field of the hippocampus (Benavides-Piccione et al. 2020) showed that the radial extent of CA1 basal arbors (~300 µm) was quite similar to that of the anterior temporal lobe. However, CA1 somata were larger than those of the temporal lobe. We believe that this maybe related to the relatively larger diameter of CA1 main apical dendrites compared to those of the temporal cortex (unpublished observations). The number of primary basal dendrites enmerging from the soma (~6 µm) was similar between these regions, as well as the distance from the soma of the maximum number of basal nodes (~40 µm) and the mean dendritic segment length per branch order (mean ± SEM. O1: 16.63 ± 0.80, O2: 48.32 ± 3.28, O3: 94.53 ± 3.69, O4: 128.90 ± 4.09, O5: 123.80 ± 6.20, O6: 145.50 ± 7.71). Thus, we found that common design principles exist and govern the patterns found in the branches that compose the basal dendrites of human neocortical and hippocampal pyramidal cells, which are different from those of the mouse cortex.

The present study also showed that layer V cells of the human temporal cortex are larger, more branched and have a greater total number of spines than those of the corresponding layer III. This is in line with previous studies in the rat and the macaque (Larkman 1991a,b; Elston 2001). However, these authors found higher, similar or lower spine density in layer III compared to layer V, depending on the classes of layer V cells sampled and the cortical region. We found a significantly higher layer III spine density at the distance from the soma of the maximum spine density (peak) compared to layer V in one individual and significantly lower layer III spine density at the peak compared to layer V in the other individual. We believe that these differences between individuals may be due to differential sampling of the various classes of layer V cells, which are known to project to different targets in experimental animals. For example, type I cells—which project to the superior colliculus, spinal cord or basal pons and are characterized by having thick tufted apical dendrites—have been described as having a higher spine density than slender (type II) layer V projection neurons, which project their axons to the contralateral hemisphere or to the ipsilateral striatum (Hübener and Bolz 1988; Matsubara et al. 1996; for review see Molnár and Cheung 2006). Whether the same is applicable to the human temporal cortex remains to be seen. However, based on previous results and unpublished observations, it seems likely that we injected, by chance, those neurons with a particularly high density of spines in one of the individuals. Thus, we support the notion that layer III cells have, as a general trend, a greater density (but lower total number) of spines than layer V. Indeed, we showed that layer III cells had a proportionally higher percentage of spines than layer V around the peak spine density in both individuals, which indicates that human layer III pyramidal cells may have a proportionally larger capacity to integrate at this particular sector of the dendritic arbor. In addition, in layer V the peak number of branches was located at approximately one-third of the radial extent of the basal arbor although the value was higher. However, the peak number of nodes was located at the same distance (40 µm) from the soma and had the same value as in layer III cells. As a result, significant differences in branching complexity were mainly found from 70 µm onwards (Supplementary Table 23). The branching angles of some of these human temporal lobe pyramidal neurons have also been analyzed in a previous work (Fernández-González et al. 2016), which showed that branching angles of layer V pyramidal cells were clearly smaller than the branching angles in layer III pyramidal cells. These different patterns between layer III and V further support the idea of intrinsic circuit variation. Finally, interareal differences have also been observed in the dendritic structure of non-human primate infragranular pyramidal neurons, similar to observations in the supragranular layers (Elston and Rosa 2000). Thus, it is probable that layer V cells of the human cortex also display interareal specialization.

In conclusion, the present data show marked differences in pyramidal cell morphology in different regions of the human temporal lobe, and among individuals, which may be important in determining the cellular and subcellular functional properties of pyramidal cells. These differences are greater and show larger inter-individual variability than those reported in other species including non-human primates. There are some characteristics of the structural design of the pyramidal cells that are systematically well-maintained, whereas there are some specific variations across cortical regions, layers and species. Thus, the similarities might be considered as basic bricks of cortical organization, whereas the differences probably indicate adaptations of the pyramidal cells to particular functions. This study emphasizes regional structural specialization as a general organizational principle in the brain.

Supplementary Material

Supplementary material can be found at Cerebral Cortex online.

Notes

We would like to thank Carmen Álvarez and Lorena Valdés for their technical assistance. We also thank Guy N Elston for his valuable comments on this manuscript, Santiago Angulo (Universidad San Pablo CEU, Madrid) for statistical assistance, and Nick Guthrie for his excellent text editing. *Competing interest:* The authors declare that they have no competing interest.

Funding

The Spanish "Ministerio de Ciencia e Innovación" (grant PGC2018-094307-B-I00); the Cajal Blue Brain Project (the Spanish partner of the Blue Brain Project initiative from EPFL, [Switzerland]); Centro de Investigación Biomédica en Red sobre Enfermedades Neurodegenerativas (CIBERNED, Spain, CB06/05/0066); and the European Union's Horizon 2020 Framework Programme for Research and Innovation (under Specific grant agreement No. 785907, Human Brain Project SGA2, and Specific grant agreement No. 945539; Human Brain Project SGA3).

References

Arion D, Sabatini M, Unger T, Pastor J, Alonso-Nanclares L, Ballesteros-Yáñez I, G Sola R, Muñoz A, Mirnics K, DeFelipe J. 2006. Correlation of transcriptome profile with electrical activity in temporal lobe epilepsy. *Neurobiol Dis*. 22:374–387.

Ballesteros-Yáñez I, Benavides-Piccione R, Bourgeois JP, Changeux JP, DeFelipe J. 2010. Alterations of cortical pyramidal neurons in mice lacking high-affinity nicotinicreceptors. *Proc Natl Acad Sci U S A*. 107:11567–11572.

Barbas H. 2015. General cortical and special prefrontal connections: principles from structure to function. *Annu Rev Neurosci*. 38:269–289.

Beaulieu-Laroche L, Toloza EHS, van der Goes M-S, Lafourcade M, Barnagian D, Williams ZM, Eskandar EN, Frosch MP, Cash SS, Harnett MT. 2018. Enhanced dendritic compartmentalization in human cortical neurons. *Cell*. 175:643–651.e14.

Benavides-Piccione R, Arellano JI, DeFelipe J. 2005. Catecholaminergic innervation of pyramidal neurons in the human temporal cortex. *Cereb Cortex*. 15:1584–1591.

Benavides-Piccione R, Fernaud-Espinosa I, Robles VC, Yuste R, DeFelipe J. 2013. Age-based comparison of human dendritic spine structure using complete three-dimensional reconstructions. *Cereb Cortex*. 23:1798–1810.

Benavides-Piccione R, Regalado-Reyes M, Fernaud-Espinosa I, Kastanauskaite A, Tapia-González S, León-Espinosa G, Rojo C, Insausti R, Segev I, DeFelipe J. 2020. Differential structure of hippocampal CA1 pyramidal neurons in the human and mouse. *Cereb Cortex*. 30:730–752.

Beul SF, Barbas H, Hilgetag CC. 2017. A predictive structural model of the primate connectome. *Sci Rep*. 7:43176.

Bianchi S, Bauernfeind AL, Gupta K, Stimpson CD, Spocter MA, Bonar CJ, Manger P, Hof P, Jacobs B, Sherwood CC. 2011. Neocortical neuron morphology in Afrotheria: comparing the rock hyrax with the African elephant. *Ann N Y Acad Sci*. 1225:37–46.

Bianchi S, Stimpson CD, Duka T, Larsen MD, Janssen WG, Collins Z, Bauernfeind AL, Schapiro SJ, Baze WB, McArthur MJ, et al. 2013. Synaptogenesis and development of pyramidal neuron dentritic morphology in the chimpanzee neocortex resembles humans. *Proc Natl Acad Sci U S A*. 110:10395–10401.

Brodmann K. 1909. In: Translated and edited by. Garey LJ, editor. *Localisation in the cerebral cortex*. London (UK): Smith-Gordon, p. 1994.

Bryant KL, Glasser MF, Li L, Jae-Cheol Bae J, Jacquez NJ, Alarcón L, Fields A, Preuss TM. 2019. Organization of extrastriate and temporal cortex in chimpanzees compared to humans and macaques. *Cortex*. 118:223–243.

Burt JB, Demirtaş M, Eckner WJ, Navejar NM, Ji JL, Martin WJ, Bernacchia A, Anticevic A, Murray JD. 2018. Hierarchy of transcriptomic specialization across human cortex captured by structural neuroimaging topography. *Nat Neurosci*. 21:1251–1259.

Chaudhuri R, Knoblauch K, Gariel MA, Kennedy H, Wang XJ. 2015. A large-scale circuit mechanism for hierarchical dynamical processing in the primate cortex. *Neuron*. 88:419–431.

DeFelipe J. 2011. The evolution of the brain, the human nature of cortical circuits, and intellectual creativity. *Front Neuroanat*. 5:29.

DeFelipe J, Fariñas I. 1992. The pyramidal neuron of the cerebral cortex: morphological and chemical characteristics of the synaptic inputs. *Prog Neurobiol*. 39:563–607.

DeFelipe J, Sola RG, Marco P, del Río MR, Pulido P, Ramón y Cajal S. 1993. Selective changes in the microorganization of the human epileptogenic neocortex revealed by parvalbumin immunoreactivity. *Cereb Cortex*. 3:39–48.

Demirtas M, Burt JB, Helmer M, Ji JL, Adkinson BD, Glasser MF, Van Essen DC, Sotiropoulos SN, Anticevic A, Murray JD. 2019. A circuit model with areal heterogeneity across cortex is fit to resting-state fMRI hierarchical heterogeneity across human cortex shapes large-scale neural dynamics. *Neuron*. 101:1181–1194.

D'Souza RD, Burkhalter A. 2017. A laminar organization for selective cortico-cortical communication. *Front Neuroanat*. 11:71.

Elston GN. 2000. Pyramidal cells of the frontal lobe: all the more spinous to think with. *J Neurosci*. 20:RC95.

Elston GN. 2001. Interlaminar differences in the pyramidal cell phenotype in cortical areas 7m and STP of the macaque monkey. *Exp Brain Res*. 138:141–152.

Elston GN. 2003. Cortex, cognition and the cell: new insights into the pyramidal neuron and prefrontal function. *Cereb Cortex*. 13:1124–1138.

Elston GN. 2007. Specializations in pyramidal cell structure during primate evolution. In: Kaas JH, Preuss TM, editors. *Evolution of nervous systems*. 1st ed. Oxford (UK): Oxford: Academic Press, pp. 191–242.

Elston GN, Benavides-Piccione R, DeFelipe J. 2001. The pyramidal cell in cognition: A comparative study in human and monkey. *J Neurosci*. 21:RC163.

Elston GN, Benavides-Piccione R, Elston A, DeFelipe J, Manger P. 2005a. Pyramidal cell specialization in the occipitotemporal cortex of the Chacma baboon (*Papio ursinus*). *Exp Brain Res*. 167:496–503.

Elston GN, Benavides-Piccione R, Elston A, Manger P, DeFelipe J. 2005b. Pyramidal cell specialization in the occipitotemporal cortex of the vervet monkey. *Neuroreport*. 16:967–970.

Elston GN, Benavides-Piccione R, Elston A, Manger P, DeFelipe J. 2011. Pyramidal cells in prefrontal cortex: comparative observations reveal unparalleled specializations in neuronal structure among primate species. *Front Neuroanat*. 5:2.

Elston GN, Manger P. 2014. Pyramidal cells in V1 of African rodents are bigger, more branched and more spiny than those in primates. *Front Neuroanat*. 8:4.

Elston GN, Rockland K. 2002. The pyramidal cell in somatosensory and motor cortex of the macaque monkey: phenotypic variation. *Cereb Cortex*. 12:1071–1078.

Elston GN, Rosa MGP. 1997. The occipitoparietal pathway of the macaque monkey: comparison of pyramidal cell morphology in layer III of functionally related cortical visual areas. *Cereb Cortex*. 7:432–452.

Elston GN, Rosa MGP. 1998. Morphological variation of layer III pyramidal neurones in the occipitotemporal pathway of the macaque monkey visual cortex. *Cereb Cortex*. 8:278–294.

Elston GN, Rosa MG. 2000. Pyramidal cells, patches, and cortical columns: a comparative study of infragranular neurons in TEO, TE, and the superior temporal polysensory area of the macaque monkey. *J Neurosci*. 20:RC117.

Elston GN, Tweedale R, Rosa MGP. 1999a. Cortical integration in the visual system of the macaque monkey: large scale morphological differences of pyramidal neurones in the occipital, parietal and temporal lobes. *Proc R Soc Lond Ser B*. 266:1367–1374.

Elston GN, Tweedale R, Rosa MGP. 1999b. Cellular heterogeneity in cerebral cortex. A study of the morphology of pyramidal neurones in visual areas of the marmoset monkey. *J Comp Neurol*. 415:33–51.

Engel J Jr. 1987. Outcome with respect to epileptic seizures. In: Engel J Jr, editor. *Surgical treatment of the epilepsies*. New York: Raven Press, pp. 553–571.

Eyal G, Mansvelder HD, de Kock CP, Segev I. 2014. Dendrites impact the encoding capabilities of the axon. *J Neurosci*. 34:8063–8071.

Eyal G, Verhoog MB, Testa-Silva G, Deitcher Y, Lodder JC, Benavides-Piccione R, Morales J, DeFelipe J, de Kock CP, Mansvelder HD, et al. 2016. Unique membrane properties and enhanced signal processing in human neocortical neurons. *Elife*. 5:e16553.

Eyal G, Verhoog MB, Testa-Silva G, Deitcher Y, Benavides-Piccione R, DeFelipe J, de Kock CPJ, Mansvelder HD, Segev I. 2018. Human cortical pyramidal neurons: from spines to spikes via models. *Front Cell Neurosci*. 12:181.

Fernández-González P, Benavides-Piccione R, Leguey I, Bielza C, Larrañaga P, DeFelipe J. 2016. Dendritic-branching angles of pyramidal neurons of the human cerebral cortex. *Brain Struct Funct*. 222:1847–1859.

Fletcher LN, Williams SR. 2019. Neocortical topology governs the dendritic integrative capacity of layer 5 pyramidal neurons. *Neuron*. 101:76–90.

Fujita I. 2002. The inferior temporal cortex: architecture, computation, and representation. *Neurocytolgy*. 31:359–371.

Garcia-Cabezas MA, Zikopoulos B, Barbas H. 2019. The structural model: a theory linking connections, plasticity, pathology, development and evolution of the cerebral cortex. *Brain Struct Funct*. 224:985–1008.

Gidon A, Zolnik TA, Fidzinski P, Bolduan F, Papoutsi A, Poirazi P, Holtkamp M, Vida I, Larkum ME. 2020. Dendritic action potentials and computation in human layer 2/3 cortical neurons. *Science*. 367:83–87.

Gilman JP, Medalla M, Luebke JI. 2017. Area-specific features of pyramidal neurons-a comparative study in mouse and rhesus monkey. *Cereb Cortex*. 27:2078–2094.

Glasser MF, Coalson TS, Robinson EC, Hacker CD, Harwell J, Yacoub E, Ugurbil K, Andersson J, Beckmann CF, Jenkinson M, et al. 2016. A multi-modal parcellation of human cerebral cortex. *Nature*. 536:171–178.

Goriounova NA, Heyer DB, Wilbers R, Verhoog MB, Giugliano M, Verbist C, Obermayer J, Kerkhofs A, Smeding H, Verberne M, et al. 2018. Large and fast human pyramidal neurons associate with intelligence. *Elife*. 7:e41714.

Hawrylycz M, Lein E, Guillozet-Bongaarts A, Shen EH, Ng L, Miller JA, van de Lagemaat LN, Smith KA, Ebbert A, Riley ZL, et al. 2012. An anatomically comprehensive atlas of the adult human brain transcriptome. *Nature*. 489:391–399.

Hübener M, Bolz J. 1988. Morphology of identified projection neurons in layer 5 of rat visual cortex. *Neurosci Lett*. 94: 76–81.

Jacobs B, Batal HA, Lynch B, Ojemann G, Ojemann LM, Scheibel AB. 1993. Quantitative dendritic and spine analyses of speech cortices: a case study. *Brain Lang*. 44:239–253.

Jacobs B, Schall M, Prather M, Kapler E, Driscoll L, Baca S, Jacobs J, Ford K, Wainwright M, Treml M. 2001. Regional dendritic and spine variation in human cerebral cortex: a quantitative study. *Cereb Cortex*. 11:558–571.

Jacobs B, Scheibel AB. 1993. A quantitative dendritic analysis of Wernicke's area in humans. I. Lifespan changes. *J Comp Neurol*. 327:83–96.

Jacobs B, Harland T, Kennedy D, Schall M, Wicinski B, Butti C, Hof PR, Sherwood CC, Manger PR. 2015. The neocortex of cetartiodactyls. II. Neuronal morphology of the visual and motor cortices in the giraffe (*Giraffa camelopardalis*). *Brain Struct Funct*. 220:2851–2872.

Jacobs B, Garcia ME, Shea-Shumsky NB, Tennison ME, Schall M, Saviano MS, Tummino TA, Bull AJ, Driscoll LL, Raghanti MA, et al. 2018. Comparative morphology of gigantopyramidal neurons in primary motor cortex across mammals. *J Comp Neurol*. 526:496–536.

Jones EG. 1984. Laminar distribution of cortical efferent cells. In: Peters A, Jones EG, editors. *Cerebral Cortex. Vol 1. Cellular components of the cerebral cortex*. New York: Plenum Press, pp. 521–553.

Kastanauskaite A, Alonso-Nanclares L, Blazquez L, Pastor J, G Sola R, DeFelipe J. 2009. Alterations of the microvascular network in sclerotic hippocampi from patients with epilepsy. *J Neuropathol Exp Neurol*. 68:939–950.

Koch C, Poggio T, Torre V. 1982. Retinal ganglion cells: a functional interpretation of dendritic morphology. *Phil Trans R Soc Lond Ser B*. 298:227–264.

Larkman AU. 1991a. Dendritic morphology of pyramidal neurones in the visual cortex of the rat. I. Branching patterns. *J Comp Neurol*. 306:307–319.

Larkman AU. 1991b. Dendritic morphology of pyramidal neurones in the visual cortex of the rat. III. Spine distributions. *J Comp Neurol*. 306:332–343.

Luebke JI. 2017. Pyramidal neurons are not generalizable building blocks of cortical networks. *Front Neuroanat*. 11:11.

Lund JS, Yoshioka T, Levitt JB. 1993. Comparison of intrinsic connectivity in different areas of macaque monkey cerebral cortex. *Cereb Cortex*. 3:148–162.

Malach R. 1994. Cortical columns as devices for maximizing neuronal diversity. *Trends Neurosci*. 17:101–104.

Marco P, Sola RG, Pulido P, Alijarde MT, Sánchez A, Ramón y Cajal S, DeFelipe J. 1996. Inhibitory neurons in the human epileptogenic temporal neocortex: an immunocytochemical study. *Brain*. 119:1327–1347.

Matsubara JA, Chase R, Thejomayen M. 1996. Comparative morphology of three types of projection-identified pyramidal neurons in the superficial layers of cat visual cortex. *J Comp Neurol*. 366:93–108.

Mohan H, Verhoog MB, Doreswamy KK, Eyal G, Aardse R, Lodder BN, Goriounova NA, Asamoah B, Brakspear AB, Groot C, et al. 2015. Dendritic and axonal architecture of individual pyramidal neurons across layers of adult human neocortex. *Cereb Cortex*. 25:4839–4853.

Molnár Z, Cheung AF. 2006. Towards the classification of subpopulations of layer V pyramidal projection neurons. *Neurosci Res*. 55:105–115.

Nakamura K, Kubota K. 1996. The primate temporal pole: its putative role in object recognition and memory. *Behav Brain Res*. 77:53–77.

Olson IR, Plotzker A, Ezzyat Y. 2007. The enigmatic temporal pole: a review of findings on social and emotional processing. *Brain*. 130:1718–1731.

Peng Y, Mittermaier FX, Planert H, Schneider UC, Alle H, Geiger JRP. 2019. High-throughput microcircuit analysis of individual human brains through next-generation multineuron patch-clamp. *Elife*. 8:e48178.

Psarrou M, Stefanou SS, Papoutsi A, Tzilivaki A, Cutsuridis V, Poirazi P. 2014. A simulation study on the effects of dendritic morphology on layer V prefrontal pyramidal cell firing behavior. *Front Cell Neurosci*. 8:287.

Rilling JK, Glasser MF, Preuss TM, Ma X, Zhao T, Hu X, Behrens TE. 2008. The evolution of the arcuate fasciculus revealed with comparative DTI. *Nat Neurosci*. 11:426–428.

Rockland KS. 2019. What do we know about laminar connectivity? *Neuroimage*. 197:772–784.

Scholtens LH, Schmidt R, de Reus MA, van den Heuvel MP. 2014. Linking macroscale graph analytical organization to microscale neuroarchitectonics in the macaque connectome. *J Neurosci*. 34:12192–12205.

Shepherd GM, Brayton RK, Miller JP, Segev I, Rinzel J, Rall W. 1985. Signal enhancement in distal cortical dendrites by means of interactions between active dendritic spines. *Proc Natl Acad Sci U S A*. 82:2192–2195.

Sola RG, Hernando-Requejo V, Pastor J, García-Navarrete E, DeFelipe J, Alijarde MT, Sánchez A, Domínguez-Gadea L, Martín-Plasencia P, Maestú F, et al. 2005. Pharmacoresistant temporal-lobe epilepsy. Exploration with foramen ovale electrodes and surgical outcomes. *Rev Neurol*. 41:4–16.

Spruston N. 2008. Pyramidal neurons: dendritic structure and synaptic integration. *Nat Rev Neurosci*. 9:206–221.

van den Heuvel MP, Scholtens LH, Feldman Barrett L, Hilgetag CC, de Reus MA. 2015. Bridging Cytoarchitectonics and Connectomics in human cerebral cortex. *J Neurosci*. 35:13943–13948.

van den Heuvel MP, Scholtens LH, de Reus MA, Kahn RS. 2016. Associated microscale spine density and macroscale connectivity disruptions in schizophrenia. *Biol Psychiatry*. 80:293–301.

Wei Y, Scholtens LH, Turk E, van den Heuvel MP. 2019. Multiscale examination of cytoarchitectonic similarity and human brain connectivity. *Netw Neurosci*. 3:124–137.

Welker C, Woolsey TA. 1974. Structure of layer IV in the somatosensory neocortex of the rat: description and comparison with the mouse. *J Comp Neurol*. 158:437–453.

White EL. 1989. *Cortical circuits: synaptic organization of the cerebral cortex. Structure, Function and Theory*. Boston: Birkhäuser.

Zilles K, Amunts K. 2010. Centenary of Brodmann's map—conception and fate. *Nat Rev Neurosci*. 11:139–145.